Supporting Information

High-Efficiency Electromagnetic Interference Shielding Capability of Magnetic $Ti_3C_2T_x$ MXene/CNT Composite Film

Luyang Liang,[a] Chao Yao,[a] Xu Yan,[b] Yuezhan Feng,*[a] Xin Hao,[a] Bing Zhou,[a] Yaming Wang,*[a] Jianmin Ma,[c] Chuntai Liu[a] and Changyu Shen[a]

[a.] *Key Laboratory of Materials Processing & Mold, Ministry of Education, National Engineering Research Center for Advanced Polymer Processing Technology, Zhengzhou University, Zhengzhou 450002, P.R. China. Email: yzfeng@zzu.edu.cn (Y. Feng), wangyaming@zzu.edu.cn (Y. Wang)*

[b.] *Beijing institute of radio measurement, China Aerospace Science and Industry Corporation Limited, Beijing, 100854, P. R. China*

[c.] *Key Laboratory for Micro-/Nano-Optoelectronic Devices, Ministry of Education, School of Physics and Electronics, Hunan University, Changsha, 410022, P.R. China*

Content:

S1: Impedance Matching ··············· **3**

S2: Electrical/Magnetic Loss Simulation Method ················ **3**

S3: EMI Shielding Efficiency ················ **4**

S4: Supplementary Figures S1-S17 ················ **5**

S5: Supplementary Tables S1 ··············· **15**

S6: Supplementary References ··············· **16**

S1: Impedance Matching

According to Eqs. (1) and (2) in manuscript, optimal impedance matching can be obtained if $Z_{in} = Z_0$ and the *RL* value tends to negative infinity. Moreover, the impedance matching can be changed *via* adjusting the composition or conductivity of absorbers. On the other hand, impedance matching can be expressed as:[1]

$$|\Delta| = \left|\sinh^2(Kfd) - M\right| \tag{S1}$$

$$K = \frac{4\pi\sqrt{\varepsilon'\mu'\sin\frac{\delta_\varepsilon + \delta_\mu}{2}}}{c\cos\delta_\varepsilon\cos\delta_\mu} \tag{S2}$$

$$M = \frac{4\mu'\varepsilon'\cos\delta_\varepsilon\cos\delta_\mu}{(\mu'\cos\delta_\varepsilon - \varepsilon'\cos\delta_\mu)^2 + \left[\tan\left(\frac{\delta_\mu}{2} - \frac{\delta_\varepsilon}{2}\right)\right]^2(\mu'\cos\delta_\varepsilon + \varepsilon'\cos\delta_\mu)^2} \tag{S3}$$

here, $\tan\delta_\varepsilon$ ($\tan\delta_\varepsilon = \varepsilon''/\varepsilon'$) and $\tan\delta_\mu$ ($\tan\delta_\mu = \mu''/\mu'$) are the abilities of dielectric and magnetic losses, respectively. In fact, smaller $|\Delta|$ value (close to zero) always represents a lower possibility of reflection, *i.e.*, a better impedance matching.

S2: Electrical/Magnetic Loss Simulation Method

COMSOL was used as the electromagnetic wave simulation software. Based on Fig. S9, a two-dimensional structure was established. Meanwhile, plane wave with a frequency of 10 GHz illuminates this structure from above in the Y-axis and a perfectly matched layer directly in the Y direction was outside the structural region. In X direction, the periodic boundary condition is used to reproduce the array mode. Due to the need of consistency between simulation and experiment, the measured frequency-dependent permittivity and permeability are imported to the corresponding structure. The wave transmission equation is shown as follows:

$$\nabla\times\mu_r^{-1}(\nabla\times E)-k_0^2(\varepsilon_r-\frac{j\sigma}{\omega\varepsilon_0})E=0 \tag{S4}$$

$$E(x,y,z)=\widetilde{E}(x,y)e^{-ik_z z} \tag{S5}$$

Among them, E is electric field intensity (N/C, V/m), K_0 is the free space wave number (rad/m), ω is the angular frequency (rad/s), σ stands for the conductivity (S/m) and ε_0 represents the vacuum dielectric constant (8.8542×10^{-2} F/m).

S3: EMI Shielding Efficiency

The EMI shielding efficiency (%) can be calculated using the equation as:[2]

$$\text{Shielding Efficiency (\%)} = 100 - \left(\frac{1}{10^{\frac{SE}{10}}}\right)\times100 \tag{S6}$$

S4: Figures S1-S17

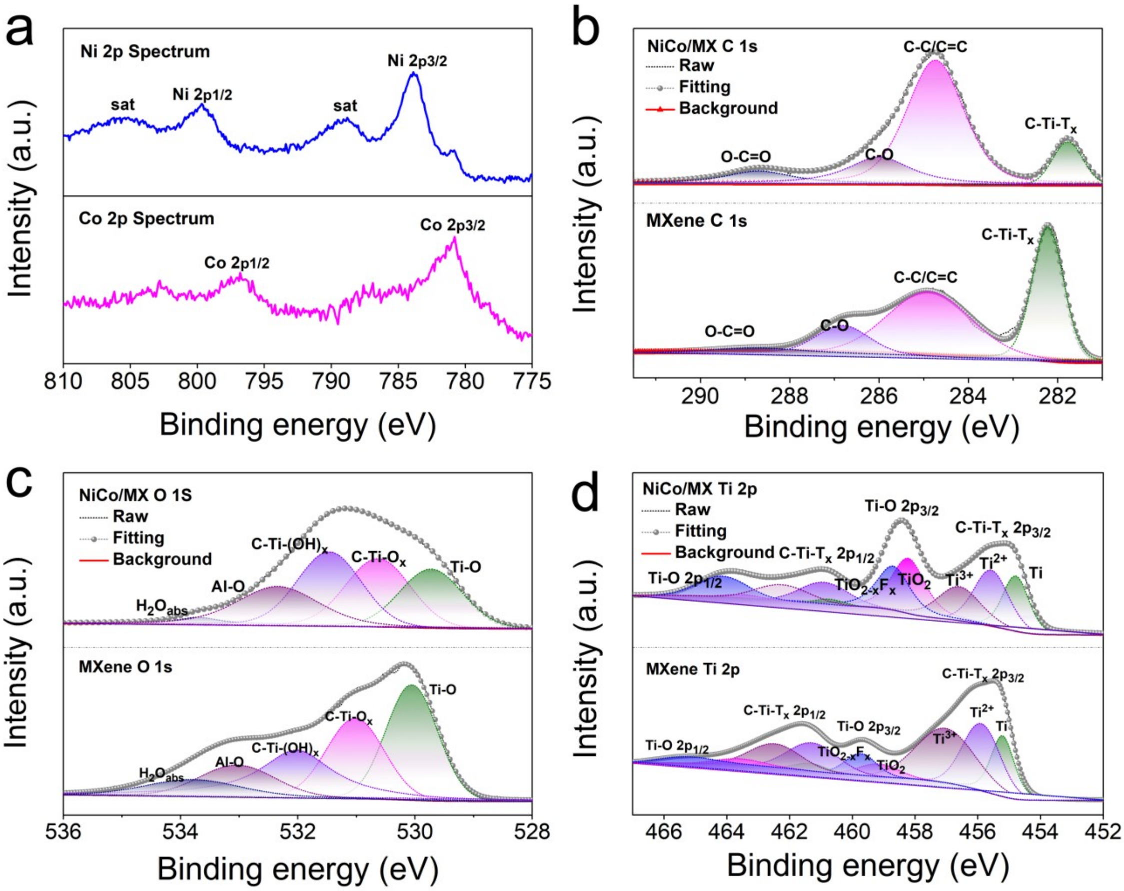

Fig. S1. High-resolution XPS spectra of $Ti_3C_2T_x$ MXene and NiCo/MX hybrid at (a) Ni 2p and Co 2p, (b) C 1s, (c) O 1s and (d) Ti 2p regions.

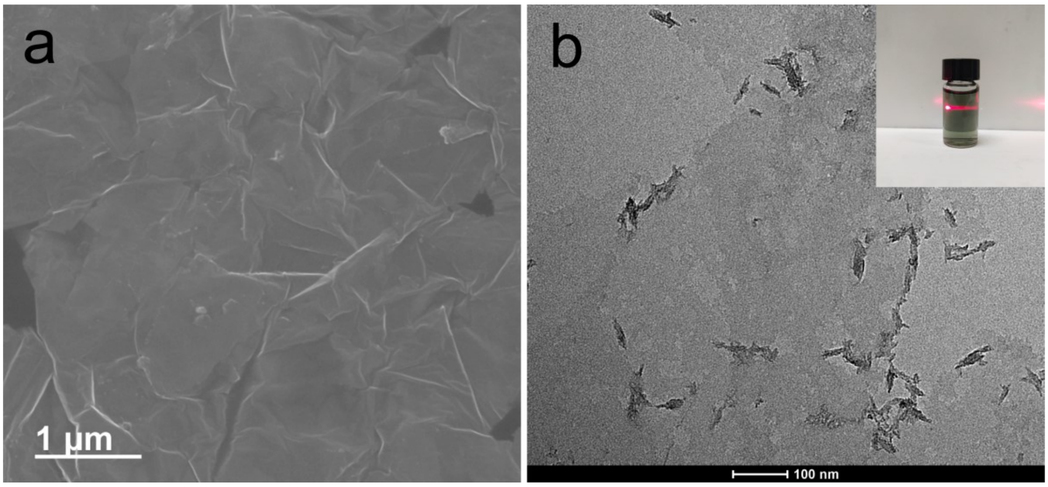

Fig. S2. (a) SEM and (b) TEM images of $Ti_3C_2T_x$ MXene and photograph of Tyndall effect (insert picture).

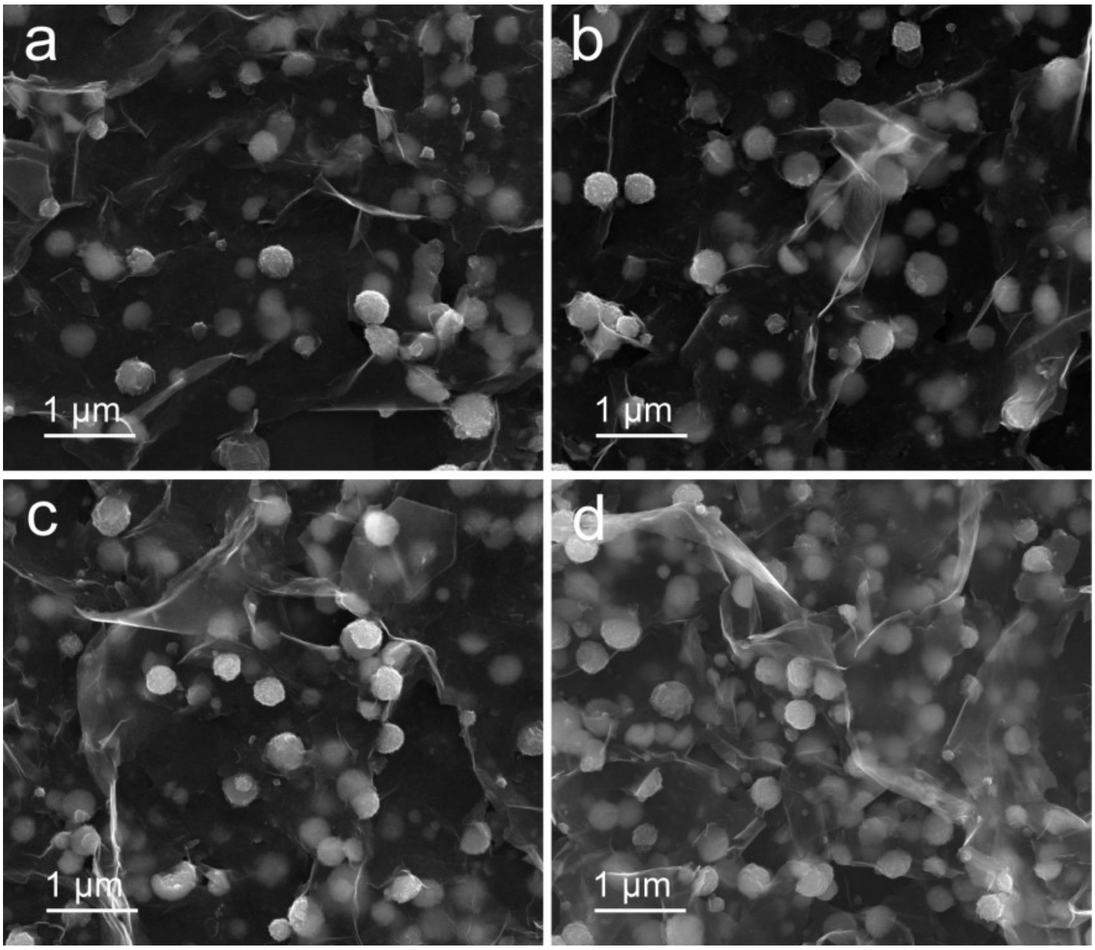

Fig. S3. SEM of (a) NiCo/MX 1:2 hybrid, (b) NiCo/MX 1:1 hybrid (c) NiCo/MX 2:1 hybrid (a) NiCo/MX 3:1 hybrid.

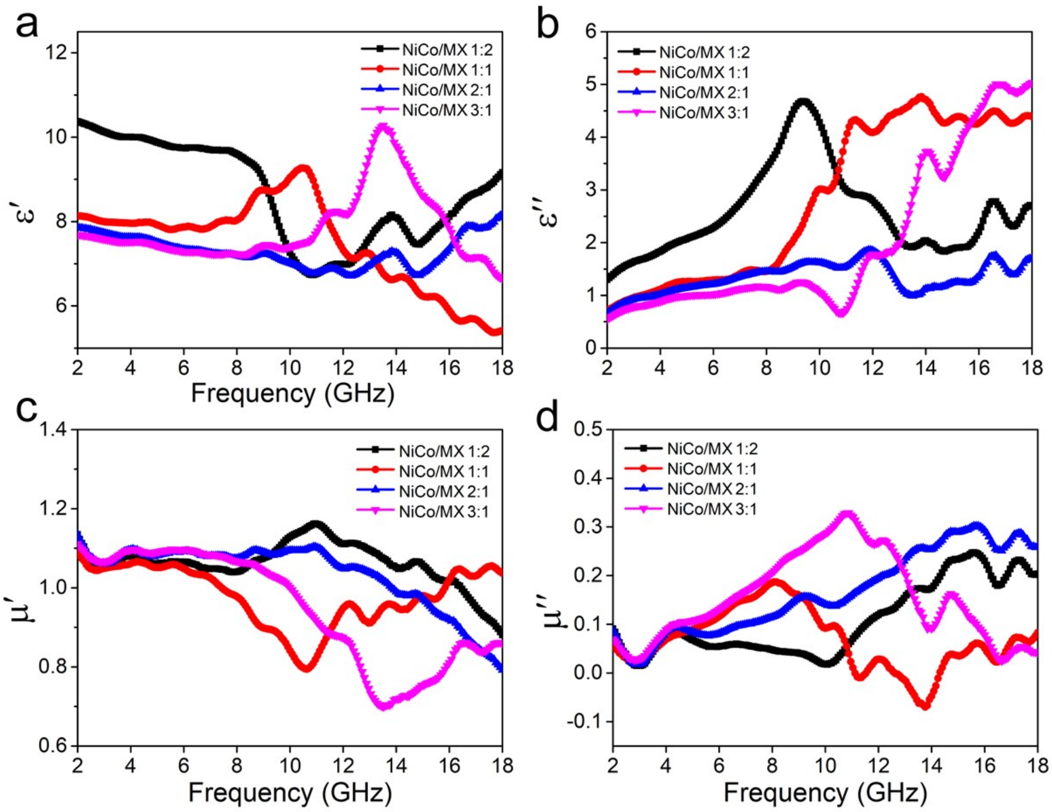

Fig. S4. Frequency dependence of (a) real and (b) imaginary parts of relative complex permittivity (ε', ε"). (c) Real and (d) imaginary parts of complex permeability (μ', μ") of NiCo/MXene hybrids with different NiCo content.

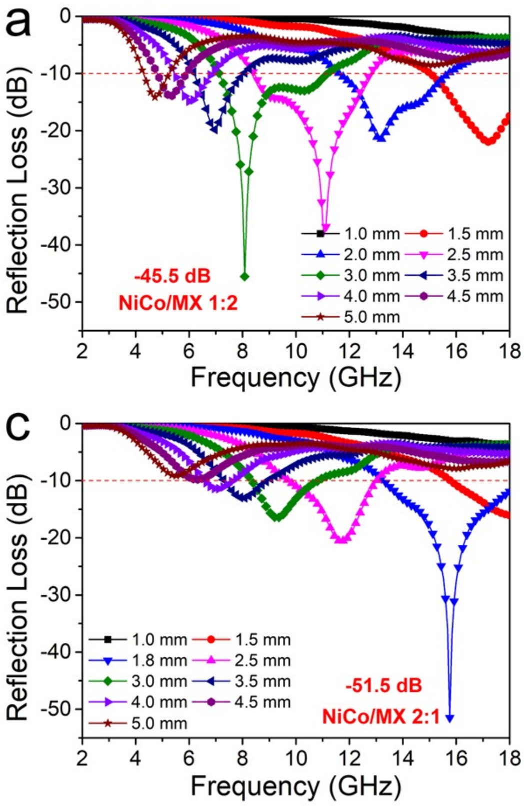

Fig. S5. Reflection loss curves of (a) NiCo/MX 1:2 hybrid, (b) NiCo/MX 1:1 hybrid (c) NiCo/MX 2:1 hybrid (a) NiCo/MX 3:1 hybrid with different thickness.

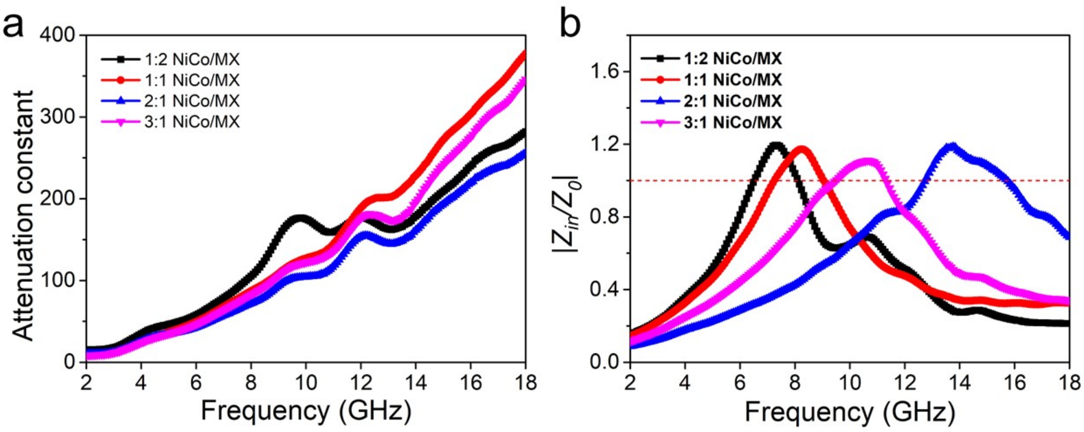

Fig. S6. (a) Attenuation constant and (b) impedance match of NiCo/MXene hybrids with different NiCo content.

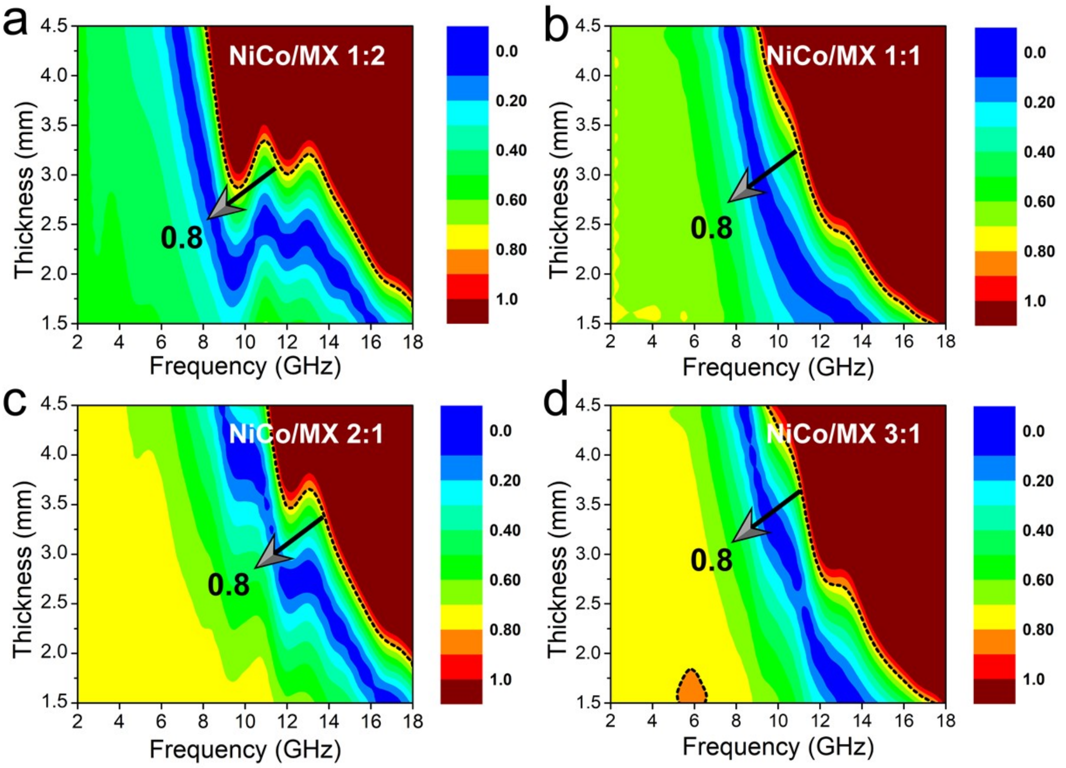

Fig. S7. Calculated │Δ│ value maps of (a) NiCo/MX 1:2 hybrid, (b) NiCo/MX 1:1 hybrid (c) NiCo/MX 2:1 hybrid (a) NiCo/MX 3:1 hybrid.

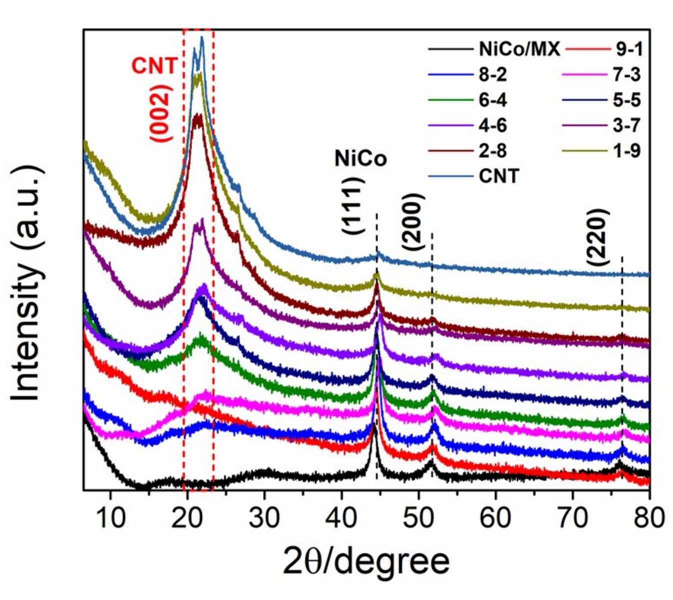

Fig. S8. XRD patterns of NiCo/MX, CNT and NiCo/MX-CNT films with different NiCo/MX:CNT ratios.

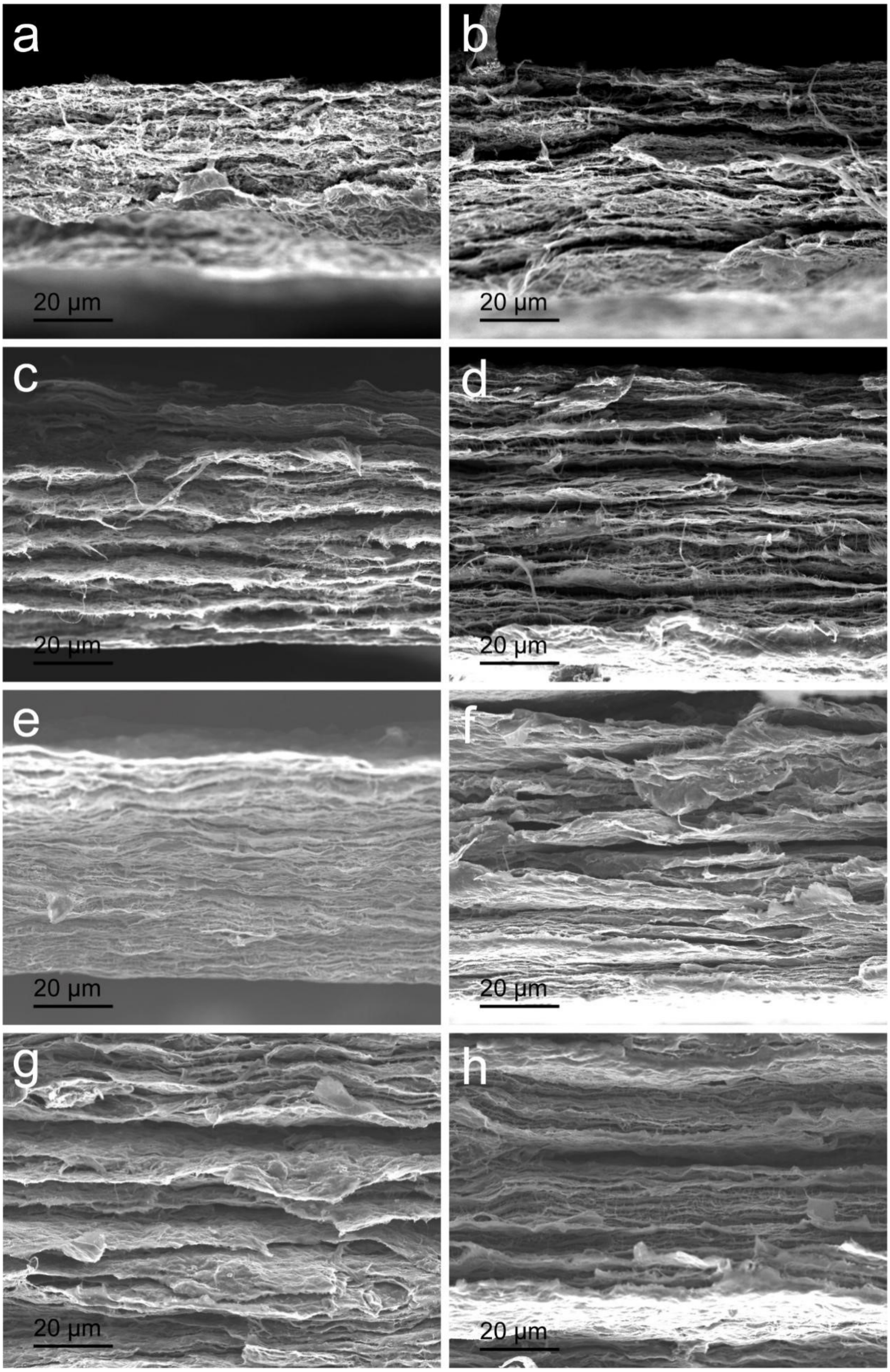

Fig. S9. Cross section SEM images of NiCo/MX-CNT film with different NiCo/MX:CNT ratio: (a) 9-1, (b) 8-2, (c) 7-3, (d) 5-5, (e) 4-6, (f) 3-7, (g) 2-8, (h) 1-9.

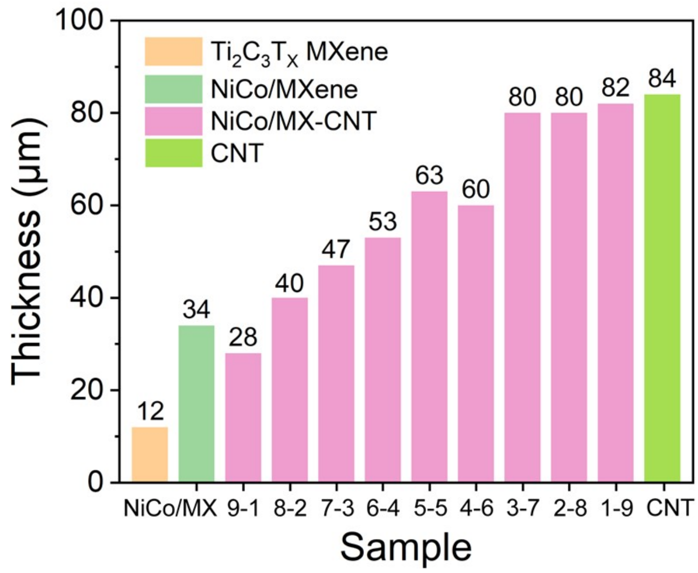

Fig. S10. Film thickness of $Ti_3C_2T_x$ MXene, NiCo/MX, CNT and NiCO/MX-CNT films with different component ratios at total mass of 50 mg.

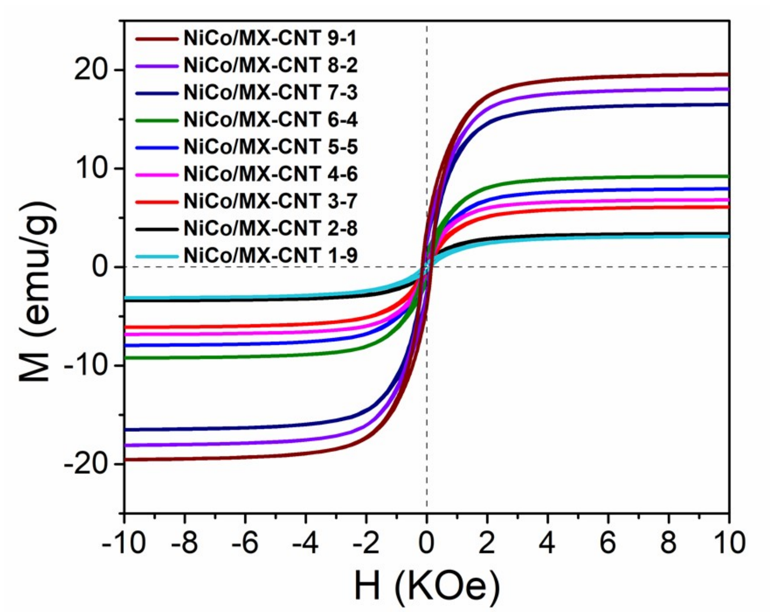

Fig. S11. VSM curves of NiCo/MX-CNT films with different component ratios.

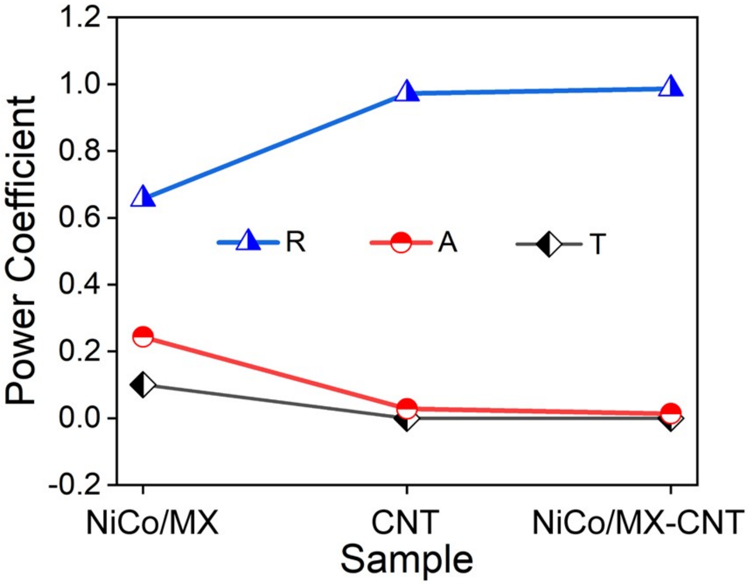

Fig. S12. R-A coefficients of NiCo/MX, CNT and NiCo/MX-CNT films.

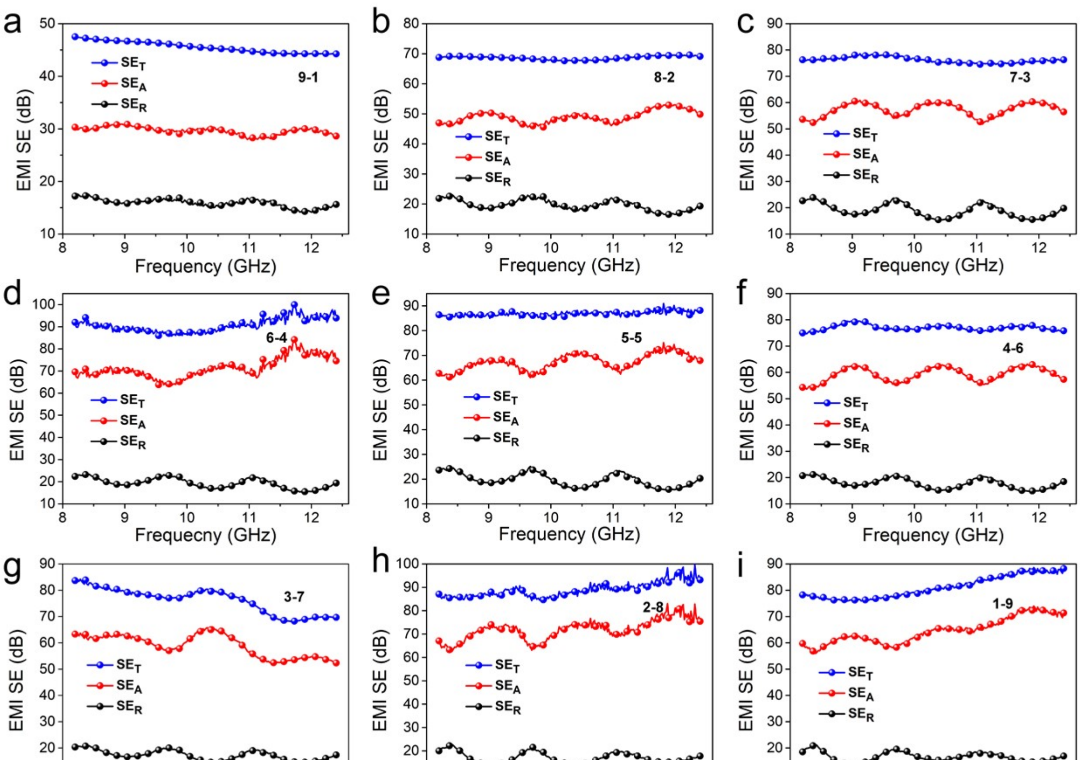

Fig. S13. EMI SET, SEA, and SER values of NiCO/MX-CNT films with different CNT ratios of (a) 9-1, (b) 8-2, (c) 7-3, (d) 6-4, (e) 5-5, (f) 4-6, (g) 3-7, (h) 2-8 and (i) 1-9.

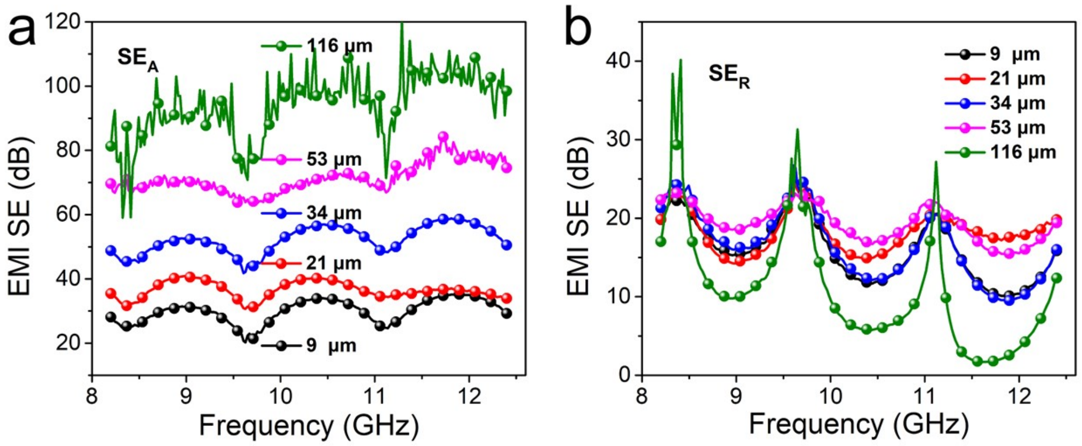

Fig. S14. EMI (a) SE_A and (b) SE_R values of NiCo/MX-CNT at different thickness.

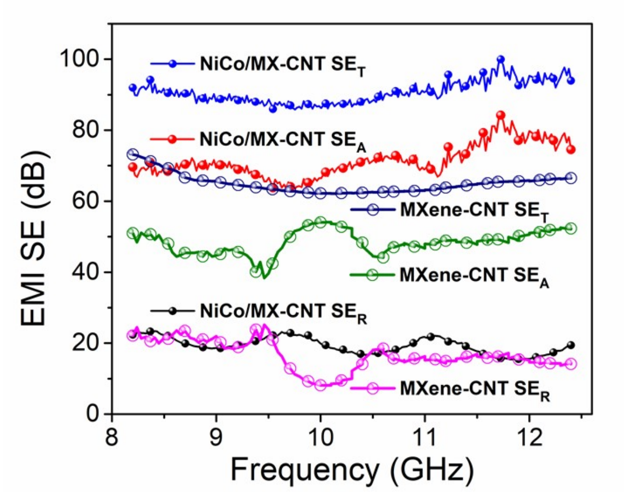

Fig. S15. EMI SE_T, SE_A, and SE_R values of NiCo/MX-CNT and MXene-CNT films.

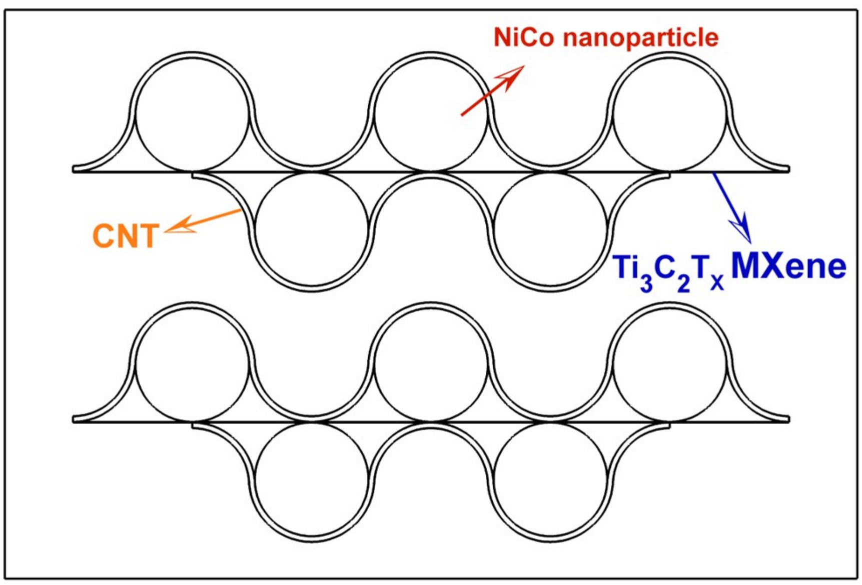

Fig. S16. Finite element model of NiCo/MX-CNT film.

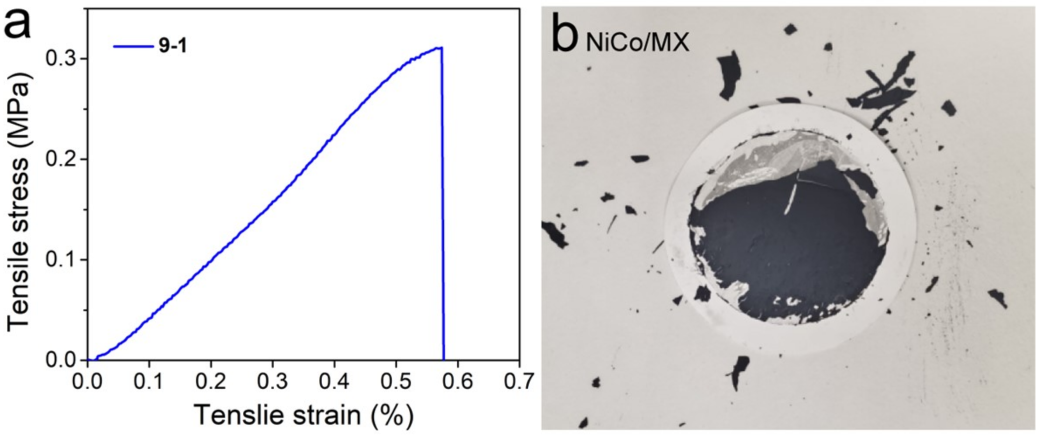

Fig. S17. (a) Tensile stress-strain curves and (b) digital photo of NiCo/MX film.

S5: Table S1 EMI shielding performance of various EMI shielding materials.

Type	Samples	Thickness [mm]	Frequency range [GHZ]	EMI SE [dB]	Conductivity [S/cm]	Ref.
Carbon fibres and tubes	CNT composite films	0.13	8-13	65	200	3
	MCMB-MWCNTs	0.6	8-12	56	11	4
	MWCNT/WPU Composites	1	8-12	21.1	/	5
	CNT sponge	1.8	8-12	54.8	/	6
	CNTs/CPE	0.5	8-12	18	0.0035	7
	CNT foam	2	8-12	33	5.16	8
	PUDA/CNT	2	8-12	30.7	0.021	9
	PEBA/MWCNT film	0.4	8-12	41	$5.6 * 10^{-4}$	10
Graphene	Graphene /CNTs	1.6	8-12	38	3.4	11
	Graphene /CNTs	1.6	8-12	36	/	12
	rGO	2	8-12	54.2	/	13
	rGO	1	8-12	38	/	14
	Expanded graphite	0.06	8-12	60.4	15	15
	RGO@AC/PVA	0.8	8-12	14	0.11	16
	Graphene foam	1.5	8-12	61	8.3	17
Metals	Ag nanowire	2.3	8-12	64	10	18
	PVDF/Ni	1.95	8-12	20	$6.19 * 10^{-6}$	19
	Epoxy/Ag-CF	2.5	8-12	35	0.8	20
	PP/Ni	3	1-12.4	20	1	21
	Stainless steel	3.1	8-12	48	/	22
Others	Carbon Foam	2	8-12	51.2	2.4	23
	MoS_2	1.5	8-12	24.2	2	24
	rGO-$BaTiO_3$	1.5	8-12	41.7	/	25
	PVA/MXene film	0.027	8-12	44.4	7.16	26
	$Ti_3C_2T_x$@Ni	2	2-18	74.17	/	27

VGSs/PI film	0.151	8–12	31.37	2.2	28
CL@GC/CE	2	8–12	35.57	32.66	29
MXene-AgNW film	0.45	8-12	27.8	/	30
MXene@Wood	10	8–12	72	0.37	31
PANI/BF	0.4	8-12	12.29	0.1	32
CCB	1.2	8-12	82	15.6	33
CNW	0.3	8-12	47	29.6	34
Mxene foam	2	8-12	62	19	35
MXene/epoxy aerogel	2	8-12	52.7	/	36
MXene/CNF paper	0.167	8-12	23	/	37
$Ti_3C_2T_x$/rGO film	0.06	8-12	59	/	38
NiCo/MX-CNT	0.009	8.2-12.4	46	1851	This work
NiCo/MX-CNT	0.053	8.2-12.4	90.7	1851	This work
NiCo/MX-CNT	0.116	8.2-12.4	105	1851	This work

S6: References

1. L. Liang, Q. Li, X. Yan, Y. Feng, Y. Wang, H.-B. Zhang, X. Zhou, C. Liu, C. Shen and X. Xie, *ACS Nano*, 2021, **15**, 6622-6632.
2. F. Shahzad, M. Alhabeb, C. B. Hatter, B. Anasori, S. Man Hong, C. M. Koo and Y. Gogotsi, *Science*, 2016, **353**, 1137-1140.
3. S. Lu, J. Shao, K. Ma, D. Chen, X. Wang, L. Zhang, Q. Meng and J. Ma, *Carbon*, 2018, **136**, 387-394.
4. A. Chaudhary, S. Kumari, R. Kumar, S. Teotia, B. P. Singh, D. A. Singh, S. Dhawan and S. Dhakate, *ACS Appl. Mater. Interfaces*, 2016, **8**, 10600-10608.
5. Z. Zeng, H. Jin, M. Chen, W. Li, L. Zhou and Z. Zhang, *Adv. Funct. Mater.*, 2016, **26**, 303-310.
6. D. Lu, Z. Mo, B. Liang, L. Yang, Z. He, H. Zhu, Z. Tang and X. Gui, *Carbon*, 2018, **133**, 457-463.
7. S. Mondal, P. Das, S. Ganguly, R. Ravindren, S. Remanan, P. Bhawal, T. K. Das and N. C. Das, *Compos. Part A Appl. Sci. Manuf.*, 2018, **107**, 447-460.
8. Y. Chen, H.-B. Zhang, Y. Yang, M. Wang, A. Cao and Z.-Z. Yu, *Adv. Funct. Mater.*, 2016, **26**, 447-455.
9. T. Wang, W.-C. Yu, C.-G. Zhou, W.-J. Sun, Y.-P. Zhang, L.-C. Jia, J.-F. Gao, K. Dai, D.-X. Yan and Z.-M. Li, *Compos. B. Eng.*, 2020, **193**, 108015.
10. G. Wang, J. Zhao, C. Ge, G. Zhao and C. B. Park, *J. Mater. Chem. C*, 2021, **9**, 1245-1258.
11. L. Kong, X. Yin, M. Han, X. Yuan, Z. Hou, F. Ye, L. Zhang, L. Cheng, Z. Xu and J. Huang, *Carbon*, 2017, **111**, 94-102.
12. Q. Song, F. Ye, X. Yin, W. Li, H. Li, Y. Liu, K. Li, K. Xie, X. Li, Q. Fu, L. Cheng, L.

Zhang and B. Wei, *Adv. Mater.*, 2017, **29**, 1701583.
13. F. Xu, R. Chen, Z. Lin, Y. Qin, Y. Yuan, Y. Li, X. Zhao, M. Yang, X. Sun, S. Wang, Q. Peng, Y. Li and X. He, *ACS Omega*, 2018, **3**, 3599-3607.
14. Y. Wu, Z. Wang, X. Liu, X. Shen, Q. Zheng, Q. Xue and J.-K. Kim, *ACS Appl. Mater. Interfaces*, 2017, **9**, 9059-9069.
15. Y. Liu, K. Zhang, Y. Mo, L. Zhu, B. Yu, F. Chen and Q. Fu, *Compos Sci Technol*, 2018, **168**, 28-37.
16. D. Lai, X. Chen, X. Liu and Y. Wang, *ACS Appl. Nano Mater.*, 2018, **1**, 5854-5864.
17. Y. Li, J. Liu, S. Wang, L. Zhang and B. Shen, *Compos. B. Eng.*, 2020, **182**, 107615.
18. Z. Zeng, M. Chen, Y. Pei, S. I. Seyed Shahabadi, B. Che, P. Wang and X. Lu, *ACS Appl. Mater. Interfaces*, 2017, **9**, 32211-32219.
19. H. Gargama, A. K. Thakur and S. K. Chaturvedi, *J. Appl. Phys.*, 2015, **117**, 224903.
20. W. Zhu, Q. Song, L. Yan, W. Zhang, P.-C. Wu, L. K. Chin, H. Cai, D. P. Tsai, Z. X. Shen, T. W. Deng, S. K. Ting, Y. Gu, G. Q. Lo, D. L. Kwong, Z. C. Yang, R. Huang, A.-Q. Liu and N. Zheludev, *Adv. Mater.*, 2015, **27**, 4739-4743.
21. S. H. Lee, J. Y. Kim, C. M. Koo and W. N. Kim, *Macromol Res*, 2017, **25**, 936-943.
22. A. Ameli, M. Nofar, S. Wang and C. B. Park, *ACS Appl. Mater. Interfaces*, 2014, **6**, 11091-11100.
23. L. Zhang, M. Liu, S. Roy, E. K. Chu, K. Y. See and X. Hu, *ACS Appl. Mater. Interfaces*, 2016, **8**, 7422-7430.
24. Q. Wen, W. Zhou, J. Su, Y. Qing, F. Luo and D. Zhu, *J. Alloys Compd.*, 2016, **666**, 359-365.
25. Q. Yuchang, W. Qinlong, L. Fa, Z. Wancheng and Z. Dongmei, *J. Mater. Chem. C*, 2016, **4**, 371-375.
26. X. Jin, J. Wang, L. Dai, X. Liu, L. Li, Y. Yang, Y. Cao, W. Wang, H. Wu and S. Guo, *Chem. Eng. J.*, 2020, **380**, 122475.
27. S. Hu, S. Li, W. Xu, W. Yu and Y. Zhou, *Ceram. Int.*, **2021**, DOI: https://doi.org/10.1016/j.ceramint.2021.07.174.
28. Z. Li, Z. Lin, M. Han, Y. Zhang and J. Yu, *ACS Appl. Nano Mater.*, 2021, **4**, 7461-7470.
29. Z. Zong, F. Ren, Z. Guo, Z. Lu, Y. Jin, Y. Zhao and P. Ren, *Compos. B. Eng.*, 2021, **223**, 109132.
30. S. Bai, X. Guo, X. Zhang, X. Zhao and H. Yang, *Compos. Part A Appl. Sci. Manuf.*, 2021, **149**, 106545.
31. M. Zhu, X. Yan, H. Xu, Y. Xu and L. Kong, *Carbon*, 2021, **182**, 806-814.
32. Y. Zhang, Z. Yang, Y. Yu, B. Wen, Y. Liu and M. Qiu, *ACS Appl. Polym. Mater.*, 2019, **1**, 737-745.
33. X. Jia, B. Shen, Z. Chen, L. Zhang and W. Zheng, *ACS Sustain. Chem. Eng.*, 2019, **7**, 18718-18725.
34. X. Ma, Y. Li, B. Shen, L. Zhang, Z. Chen, Y. Liu, W. Zhai and W. Zheng, *ACS Appl. Mater. Interfaces*, 2018, **10**, 38255-38263.
35. X. Wu, B. Han, H.-B. Zhang, X. Xie, T. Tu, Y. Zhang, Y. Dai, R. Yang and Z.-Z. Yu, *Chem. Eng. J.*, 2020, **381**, 122622.
36. S. Zhao, H.-B. Zhang, J.-Q. Luo, Q.-W. Wang, B. Xu, S. Hong and Z.-Z. Yu, *ACS Nano*, 2018, **12**, 11193-11202.
37. W.-T. Cao, F.-F. Chen, Y.-J. Zhu, Y.-G. Zhang, Y.-Y. Jiang, M.-G. Ma and F. Chen, *ACS Nano*, 2018, **12**, 4583-4593.
38. Y. Zhang, K. Ruan, X. Shi, H. Qiu, Y. Pan, Y. Yan and J. Gu, *Carbon*, 2021, **175**, 271-280.